Determining the thermophysical properties of Al-doped ZnO nanoparticles by the photoacoustic technique*

T. A. El-Brolossy[a)b)†], O. Saber[a)c)], and S. S. Ibrahim[a)d)]

[a)] Department of Physics, Faculty of Science, King Faisal University, Al-Ahsa, Saudi Arabia
[b)] Department of Physics, Faculty of Science, Ain Shams University, Cairo, Egypt
[c)] Egyptian Petroleum Research Institute, Cairo, Egypt
[d)] Department of Physics, Faculty of Science, Cairo University, Giza, Egypt

(Received 5 November 2012; revised manuscript received 15 January 2013)

The thermal conductivity and specific heat capacity of undoped and Al-doped (1–10 at.%) ZnO nanoparticles prepared using the solvent thermal method are determined by measuring both thermal diffusivity and thermal effusivity of a pressed powder compact of the prepared nanoparticles by using the laser-induced photoacoustic technique. The impact of Al doping versus the microstructure of the samples on such thermal parameters has been investigated. The results reveal an obvious enhancement in the specific heat capacity when decreasing the particle size, while the effect of Al doping on the specific heat capacity is minor. The measured thermal conductivities are about one order of magnitude smaller than that of the bulk ZnO due to several nested reducing heat transfer mechanisms. The results also show that Al doping significantly influences the thermal resistance. Using a simple thermal impedance model, the added thermal resistance due to Al dopant has been estimated.

Keywords: ZnO nanoparticles, microstructure, specific heat, thermal conductivity

PACS: 44.30.+v, 44.10.+i, 65.80.–g, 66.10.cd **DOI:** 10.1088/1674-1056/22/7/074401

1. Introduction

Searching for materials with tunable and new thermal, electrical, and mechanical properties is considered as the most important motivation for many researchers in recent years. Knowledge of thermophysical properties, especially thermal conductivity, is essential in many applications involving heat generation or high temperature. In some applications such as electronic devices, the lower the thermal conductivity in some points, the hotter the device. On the other hand, low thermal conductivity is essential for enhanced energy conversion efficiency in thermoelectric applications. Thermal conductivity and heat capacity of a solid determine whether homogeneous temperature is achieved quickly during the firing cycle. When the dimensions of the material are reduced to the nanometer level, the interface effect can be a dominant factor in light of 10^{19} or more interfaces per cm^3. In general, the interface/grain boundary provides an effective way to scatter phonons and subsequently lower the thermal conductivity.

As one of the most important metal oxides, ZnO possesses a direct wide band gap (3.5 eV) and large exciton binding energy of 60 meV.[1] Based on these properties, it has gained a great interest in electrical, optical, and magnetic applications.[2–5] ZnO nanostructures also have been widely used in various applications such as solar cells,[6] gas sensors,[7] piezoelectric devices,[8] and biomaterials.[9]

It is well known that intrinsic and extrinsic dopants represent a feasible route to modify optical, electrical, and thermal properties of materials and a practicable way to improve their thermoelectric performance. It has been recognized that a small amount of Al doping increases electrical conductivity by more than 3 orders of magnitude at room temperature.[10] Doped ZnO, especially Al-doped ZnO is one of the best n-type thermoelectric oxide materials reported to date.[11] Several reports[12–16] have studied the effect of doping with metals (Al^{3+}, In^{3+}, Ga^{3+}, etc.) on the microstructure, electrical and optical properties of ZnO. Despite the thermal properties of such materials being worthy of close scrutiny from a device design point of view, thermophysical characterization of such systems have been rarely studied. A number of researchers exerted sensible efforts in studying thermal properties of undoped ZnO nanoparticles and/or thin films under the influence of temperature.[17–20]

Microstructural factors can also have a significant influence on the measured thermal properties of a sample. Pores, filled with gas of a lower thermal conductivity than the solid phase, help block the heat flow and thus make the material more insulating. Interfaces such as grain boundaries, which are crossed by the heat flow path, can also inhibit heat conduction. In this work, the impact of lightly and heavily Al doping (0–10 at.%) versus microstructure on the thermophysical properties of green ZnO nanoparticles has been investigated.

The thermal diffusivity, α ($cm^2 \cdot s^{-1}$) is a significant thermophysical parameter which measures how effectively

*Project supported by the Deanship of Scientific Research, King Faisal University, Saudi Arabia (Grant No. 130154).
†Corresponding author. E-mail: taali@kfu.edu.sa; elbrolosyta@yahoo.com
© 2013 Chinese Physical Society and IOP Publishing Ltd

phonons carry heat through the sample. Whereas measurement of the heat exchange rate or the thermal impedance for heat exchange of a given material is essentially determined by its thermal effusivity e (in unit of $\mathrm{W{\cdot}s^{1/2}{\cdot}cm^{-2}{\cdot}K^{-1}}$), which is a relevant thermophysical parameter for surface heating or cooling processes as well as in quenching processes. These quantities are defined by $\alpha = k/\rho c$ and $e = (k\rho c)^{1/2}$, where k is the thermal conductivity, c is the specific heat capacity, and ρ is the mass density. With α and e known, the sample thermal conductivity and volume heat capacity C (=ρc) can be obtained through the relations $k = e\sqrt{\alpha}$ and $C = e/\sqrt{\alpha}$, respectively. Specific heat capacity is one of the fundamental thermodynamic data of materials and is very important to many physical and chemical researches and engineering technology design concerned with materials. Many other thermodynamic properties, such as enthalpy, entropy, and Gibbs free energy can be calculated from highly precise heat capacity data.[21]

Recently, thermal wave physics has been emerging as a respected tool for optical and thermal characterization of materials in all its different forms. Absorption of intensity modulated optical radiation by a sample leads to periodic heat generation, thereby causing excitation of thermal waves in the specimen. Among various methods used to study these thermal waves, the laser induced photoacoustic (PA) technique is one of the most commonly employed experimental approaches. Therefore, because it is noncontact and nondestructive, the PA method has gained more popularity due to the versatility in employing different configurations to measure the required thermophysical parameters with great accuracy. The PA technique has two different configurations: heat reflection configuration (Fig. 1(a)) where the illumination and detection of the signal are from the same side of the sample, and heat transmission configuration (Fig. 1(b)) where the illumination is at the front surface whereas the signal is detected at the rear surface. In particular, heat transmission configuration is becoming increasingly popular for thermal diffusivity evaluation,[22,23] while thermal effusivity is measured usually through reflection configuration,[24,25] utilizing a reference sample of known e.

Assuming the sample is optically opaque (i.e., the whole modulated energy is absorbed at the surface) and thermally thick (i.e., thermal diffusion length is much smaller than the thickness of the sample), the PA signal amplitude (q) in the heat transmission configuration is given by[26]

$$q = A\frac{1}{f}\exp\left(-\frac{\pi^{1/2}f^{1/2}l}{\alpha^{1/2}}\right), \tag{1}$$

where f is the modulation frequency, ℓ is the thickness of the sample, and A is a constant containing the thermal effusivity of the sample with unrelated sample constants. This relation is usually used to determine α of the sample of known thickness ℓ from the slope of $\ln(qf)$ as a function of $f^{1/2}$. In heat reflection configuration, the PA signal of optically opaque and thermally thick samples is given by[27]

$$q = \frac{A^*}{ef}, \tag{2}$$

where A^* is a irrelated sample constant. This relation can be used to estimate effusivity of the tested samples using a standard material of known effusivity under the same conditions, where the constant A^* can then be eliminated.

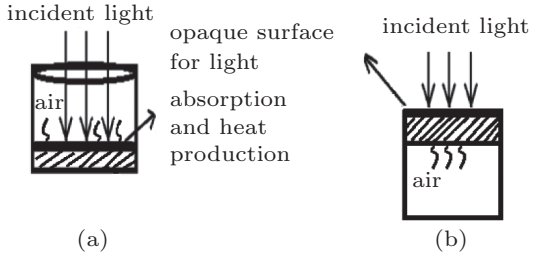


Fig. 1. Schematic diagram of (a) heat reflection and (b) heat transmission configurations.

2. Experimental details

Undoped and Al-doped (1, 3, 5, 10 at.%) ZO nanoparticles have been prepared using the solvent thermal technique.[28] This technique has been successfully applied for the synthesis of various types of nanosized metal oxides with large surface area, high crystallinity, and high thermal stability. A detailed account of the preparation conditions for the present samples has been given in Ref. [29]. Zinc acetate was used as zinc precursor and the solvent was methanol. The solution after continuous stirring for 12 h was placed in a pressurized vessel with a temperature controller. The dehydroxylation and drying processes were achieved under supercritical conditions (250 °C, 70 bar) in the presence of ethanol (350 mL). Al-doped ZO nanoparticles with different concentrations of Al were prepared by adding appropriate amounts of aluminum nitrate during the preparation of ZO.

Complete characterizations of the prepared samples have been performed previously,[29] where the nanoscale of doped and undoped ZnO was confirmed using scanning and transmission electron microscopy. Also, powder X-ray diffraction (XRD) spectra were recorded on Rigaku, RINT 22002200 using CuKα (filtered) radiation ($\lambda = 0.154$ nm). The X-ray diffraction pattern of ZnO particles (Fig. 2(a)) exhibits the high crystallinity of the wurtzite hexagonal structure with considerably broadened diffraction lines, indicating the nanoscale crystallinity of the ZnO particles with randomly oriented polycrystalline. The mean crystallite size of the ZnO particles estimated from XRD pattern is about 37 nm. By doping ZnO particles with different concentrations of Al, no new peaks are formed for the Al-doped ZnO samples as shown in Fig. 2(b) that shows the XRD patterns of lowest and highest Al-doped

samples. In addition, all diffraction peaks of the zincite phase were observed for all samples with high crystallinity. This means Al may be homogeneously dispersed inside the wurtzite structure of ZnO or it has an amorphous form. Furthermore, the Al doping of ZnO particles slightly affects the nanometer size of ZnO crystals. It is worthy noted that, low Al concentrations (1 at.% and 3 at.%), result in lower crystallite sizes (31 nm and 31.4 nm). On the other hand, higher Al concentrations (5 at.% and 10 at.%) lead to higher crystallite sizes (38.7 nm and 42.8 nm). This may be due to two competing effects. First, we know that the atomic weight of Al (27) is lower than that of Zn (65). Then, it is expected that the inclusion of Al instead of Zn decreases the particle size of the crystal. Second, as Al is tri-valent (+3) whereas Zn is di-valent (+2), Al needs more oxygen than Zn for neutralization. Therefore, inclusion of Al instead of Zn may lead to an increase in the particle size. For low Al concentrations, the last effect is not clear because of the good dispersion of Al in the ZnO matrix and the first effect is predominant. On the other hand, the second effect becomes much more significant for high Al concentrations.

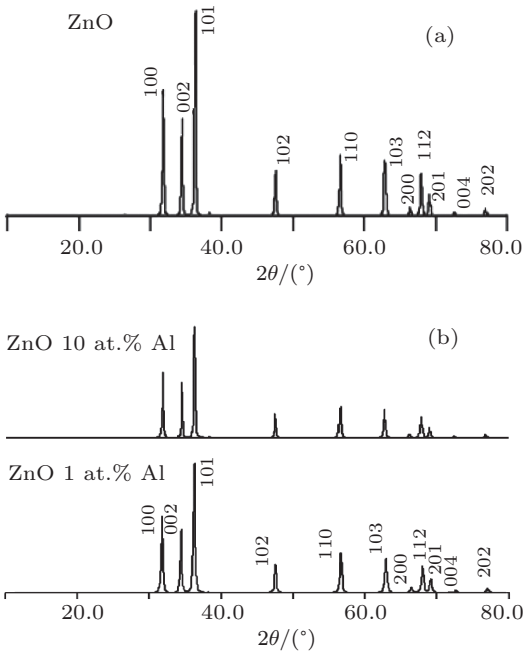


Fig. 2. (a) X-ray diffraction patterns of the prepared ZnO. (b) X-ray diffraction patterns of the prepared Al-doped ZnO (lowest and highest Al concentrations).

The differential scanning calorimetric analysis of the powdered samples shows that the ejection of all organics was completed at about 320 °C, and therefore the samples were calcined at 320 °C. ZnO nanopowders were uniaxially pressed at room temperature to disc pellets of 10 mm in diameter and 1 mm in thickness, applying a force of 5 tons. Care was taken to pelletize all the samples at identical experimental conditions. The thicknesses of the specimens used in the present investigation were further reduced to ~ 400 μm. The porosity (p) of the sample was evaluated using the formula $p = 1 - (\rho_{\rm m}/\rho_{\rm th})$,[30] where $\rho_{\rm m}$ is the measured density (using geometrical dimension and mass) while $\rho_{\rm th}$ is the theoretical density. Table 1 gives Al concentration, average particle size, and porosity of the samples used in this investigation. As expected, the results show that the particle size has the predominant effect on the sample porosity; the highest porosities are for samples of the smallest particles. For samples of comparable particle size, slight increase in porosity with increasing Al concentration is obtained. PA measurements were carried out by gas-microphone detection method. A detailed account of the present experimental set-up can be found elsewhere.[31,32] The PA cell (0.5 $\rm cm^3$) is made of stainless steel and anodized Al. It includes a built-in microphone with a sensitivity of 50 mV/Pa in addition to a preamplifier. The cell is designed for high signal to noise ratios and acoustic vibration. The cell is sealed with rubber O-rings at the sample holder and microphone outlet. The window of the sample carrier is available in several materials to cover the UV–Vis–IR ranges. A continuous wave laser at 514.53 nm from an Ar laser is used as the excitation beam. Laser power of 20 mW is employed for the measurements. A mechanical chopper is used to modulate the pump beam at the desired frequency (f) for thermally thick samples. Crystalline Si of well-known thermal parameters is used as a reference sample for thermal effusivity measurements. Before measurements, both reference and test samples were coated with a very thin layer of carbon black to produce equivalent optical absorption on the surfaces of the samples, which is a critical requirement for accurate effusivity determination. It also enhances the signal to noise ratio in diffusivity measurements. The amplitude of the signal as a function of modulation frequency of the laser beam is recorded using a dual-channel digital lock-in amplifier (SR830).

3. Results and discussion

The experimental results of PA signal amplitude in heat transmission configuration as a function of modulation frequency were obtained first. The measurements were performed to calculate α in the frequency region where the samples are thermally thick as required by Eq. (1). The relation between $\ln(qf)$ and $f^{1/2}$ for undoped samples is shown in Fig. 3(a) together with two Al-doped ZnO samples (1 and 10 at.%). The experimental points were fitted by straight lines according to Eq. (1). The other two specimens show similar behavior (not shown). Thermal diffusivity values of all samples were directly obtained from the slope of the fitted lines using the thickness of the samples as a known parameter. Figure 3(b) shows the variation of the signal amplitude with the inverse of modulation frequency in the heat reflection configuration for the same samples together with the crystalline Si sample as a reference of known effusivity

(1.567 $W{\cdot}s^{1/2}{\cdot}cm^{-2}{\cdot}K^{-1}$). The constant A in Eq. (2) can be eliminated by normalizing the signal of the sample under investigation to that of the reference and as a result, thermal effusivity of all samples can be determined.

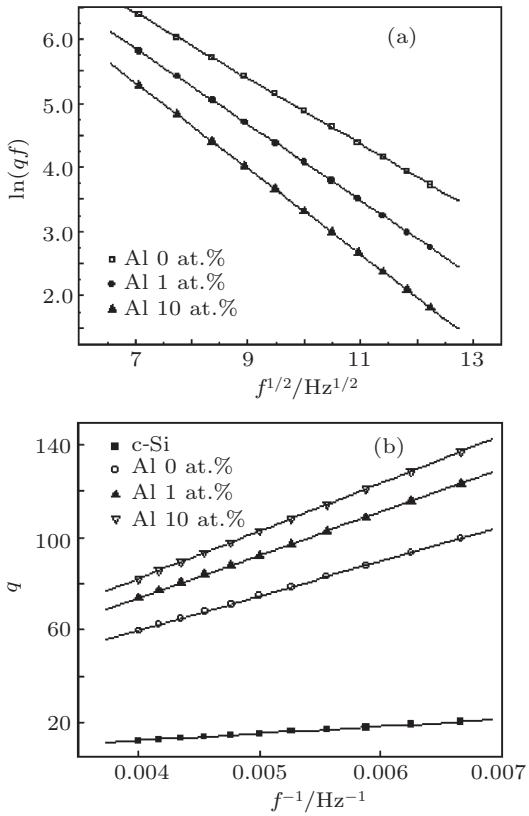


Fig. 3. (a) PA measurements of $\ln(qf)$ versus $f^{1/2}$ in heat transmission configuration for the undoped ZnO sample together with two Al-doped samples. (b) PA signal in heat reflection configuration versus f^{-1} for the c-Si together with the undoped and doped ZnO samples.

The obtained values for both α and e are given in Table 1. It is clear that these values in case of Al-doped samples are lower than those of the undoped sample. However, the change in both α and e with increasing Al concentration is irregular. These results can be understood in terms of the definition of e and α as derived quantities related to both k and C. As a result, they depend upon the microscopic structure and various imperfections of the material such as impurity, porosity, and grain boundary.

The values of α and e have been used to calculate both the effective thermal conductivity k_m $(= e\sqrt{\alpha})$ and volume heat capacity C $(= e/\sqrt{\alpha})$ for all samples which are listed in Table 1. As shown in Table 1, the values of C for all tested samples are smaller than that of the bulk dense polycrystalline ZnO, i.e., around 2.82 $J{\cdot}cm^{-3}{\cdot}K^{-1}$.[33] More than one parameter can affect the measured values of C of the pressed nanopowder compact materials. This can be illustrated in the following. The lowest value of C is for 3 at.% Al-doped ZnO sample which has the highest porosity while its highest value is for the undoped ZnO sample of least porosity. This reflects the direct proportionality of C to the density ρ_m of the samples. Also the particle size may play an important role in controlling the value of C through its effect on the specific heat capacity c (in unit of $J{\cdot}g^{-1}{\cdot}K^{-1}$). It has been proved experimentally that the specific heat capacity of nanoparticles exceeds that of analogous bulk materials.[34,35] Our results agree with such findings as can be seen in Fig. 4 that shows the ratio of specific heat c $(= C/\rho_m)$ measured for all ZnO nanoparticles under study to that of the bulk ZnO ($c_o \approx 0.48$ $J{\cdot}g^{-1}{\cdot}K^{-1}$). This relation confirms that the enhancement of specific heat decreases with increasing particle size.

Table 1. Thermal diffusivity, effusivity, and conductivity with the volume heat capacity of ZnO of different Al concentrations.

Al Conc. /at.%	Particle size/nm	Porosity /%	α /10^{-3} $cm^2{\cdot}s^{-1}$	e /$W{\cdot}s^{1/2}{\cdot}cm^2{\cdot}K^{-1}$	k_m /10^{-2} $W{\cdot}cm^{-1}{\cdot}K^{-1}$	C /$J{\cdot}cm^{-3}{\cdot}K^{-1}$
0	37	20	19.13	0.318	4.40	2.30
1	31	28.9	14.32	0.257	3.07	2.15
3	31.4	30.3	11.51	0.226	2.43	2.11
5	38.7	21	11.95	0.246	2.69	2.25
10	42.8	22.6	11.23	0.231	2.45	2.18

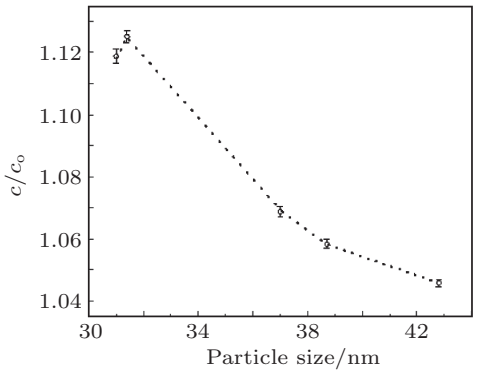


Fig. 4. Specific heat ratio (c/c_o) as a function of particle size.

Several factors associated with reducing the size can be responsible for such anomalous behavior of specific heat capacity of nanoparticles. One of these factors is the contribution of the surface free energy to the total energy of the system.[36] This contribution could be essential for nanocrystals with a comparable number of bulk and surface atoms. Also, the increase in the configuration and vibrational entropy of grain boundaries can lead to heat capacity enhancement in the nanostructured materials. Other factors such as the excess volume, reduction in density, and increase in specific surfaces[37] may help to improve the specific heat capacity. Al-

though slight impurity can enhance the heat capacity[38] (this appears for samples 3 at.% Al and 1 at.% Al of nearly equal particle size, ~ 31 nm), the predominant effect on the specific heat capacity in our results is the particle size.

It can be seen from Table 1 that the measured thermal conductivity of all ZnO nanoparticles (doped and undoped) are much smaller than those of the bulk single crystal ZnO which is around 0.54 W/(cmK).[20] Obviously, the samples under study contain a number of nested factors such as particle size, porosity, impurity, and defects. Hence, the measured thermal conductivity contains contributions from different heat diffusion mechanisms. The dependence of thermal conductivity on grain size usually results from grain boundary that causes phonon scattering, which may reduce the phonon mean free path, and at the same time, introduce extra boundary thermal resistance. Using a similar approach for ac impedance studies, the thermal conductivity of the dense polycrystalline materials k_s can be described by the following equation:[39]

$$\frac{1}{k_s} = \frac{1}{k_b} + \frac{r}{D} + \Delta R, \tag{3}$$

where k_b is the thermal conductivity of pure single crystal, r is the grain boundary thermal resistance, D is the grain size, and ΔR is the thermal resistivity produced by impurity and defects. It is clear that the porosity effect which plays an important role in controlling thermal conductivity of porous media is not included in Eq. (3) that deals with dense media. In order to take the porosity effect into account, effective medium expression[40] for materials containing randomly dispersed pores can be used to describe the effective thermal conductivity.[41] This is given by

$$k_m = \frac{1}{4}\left[k_p(3\phi - 1) + k_s(2 - 3\phi) + \left\{\left[k_p(3\phi - 1) + k_s(2 - 3\phi)\right]^2\right\}^{1/2} + 8k_s k_p\right], \tag{4}$$

where k_s is the solid phase thermal conductivity, k_p is the thermal conductivity of the pore phase, and ϕ is the porosity percentage. Equation (4) can be used to calculate k_s that can be fed into Eq. (3) to calculate ΔR. Assuming r ($\approx 0.87 \times 10^{-9}$ m^2·K·W^{-1}) is independent of grain size[20] and the thermal conductivity of single crystal ZnO is 54 W·m^{-1}·K^{-1} at room temperature, the values of ΔR can be obtained. The results show that the thermal resistivity due to impurity and defects is the least for undoped ZnO sample ($\Delta R_o = 0.117$ mK·W^{-1}) and increases with increasing Al concentrations. The impact of Al doping specifically on the added thermal resistivity of ZnO nanoparticles can be highlighted by plotting the increase in thermal resistance ($\Delta R - \Delta R_o$) as a function of Al concentration, as shown in Fig. 5. This indicates the reduction of thermal conductivity with increasing Al dopants. Since the thermal conductivity of the material is actually the sum of phonon thermal conductivity and electron thermal conductivity, the above results can be understood in terms of dominant phonon contribution. The addition of dopants adds to the scattering of the phonon, resulting in reduction in the phonon thermal conductivity. However, for the highest Al-doping sample (10 at.%) the electronic thermal conductivity becomes more significant, and partially compensates for the reduction in phonon contribution due to scattering.

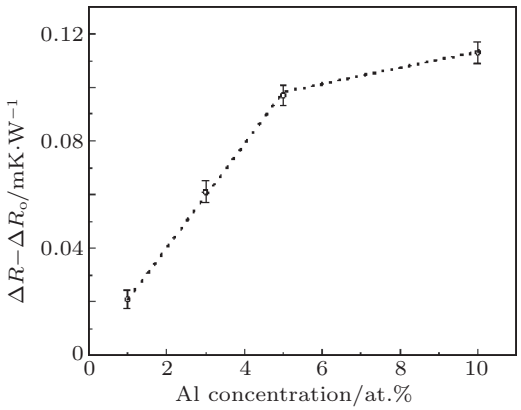


Fig. 5. The increase in thermal resistance ($\Delta R - \Delta R_o$) as a function of Al doping concentration.

4. Conclusion

Thermal properties including diffusivity, effusivity, conductivity, and specific heat capacity of undoped and Al-doped (1–10 at.%) ZnO nanopowder compact are obtained using PA technique. Several microstructure factors such as porosity, grain size and/or boundary, impurity and defects in addition to the Al doping can affect heat transfer in such samples. In this study, we are able to investigate the impact of each of these factors on thermal properties of ZnO nanoparticles. An obvious enhancement in the specific heat capacity of ZnO nanoparticles with respect to that of ZnO bulk has been detected. The results reveal that specific heat capacity depends mainly on the average particle size and to a lesser extent on the Al doping concentration. On the other hand, the measured thermal conductivity of nanoparticles is much smaller than that of the bulk ZnO and decreases with increasing Al doping concentration. Using simple analysis the role of Al doping in increasing thermal resistance has been estimated. These results disclose the capability of this simple noncontact and nonintrusive technique to detect variations of thermal parameters of such polycrystalline materials due to several nested heat transfer aspects.

References

[1] Yoshinari A, Ishida K, Murai K and Moriga T 2009 *Mater. Res. Bull.* **44** 432
[2] Sedky A and El-Suheel E 2012 *Chin. Phys. B* **21** 116103
[3] Lupan O, Pauport'e T and Viana B 2010 *J. Phys. Chem. C* **114** 14781

[4] Yao Y H and Cao Q X 2012 *Chin. Phys. B* **21** 124205

[5] Pan F, Guo Y, Cheng F F, Fa T and Yao S D 2011 *Chin. Phys. B* **20** 127501

[6] Zhang Q, Dandeneau C S, Zhou X and Cao G 2009 *Adv. Mater.* **21** 4087

[7] Lupan O, Ursaki V, Chai G, Chow L, Emelchenko G A, Tiginyanu I M, Gruzintsev A N and Redkin A N 2010 *Sensor. Actuat. B* **144** 56

[8] Wang X, Song J, Liu J and Wang Z L 2007 *Science* **316** 102

[9] Lee J, Kang B S, Hicks B, Chancellor T F, Chu B H, Wang H T, Keselowsky B G, Ren F and Lele T P 2008 *Biomaterials* **29** 3743

[10] Ohtaki M, Tsubota T, Eguchi K and Arai H 1996 *J. Appl. Phys.* **79** 1816

[11] Cheng H, Xu X J and Hng H H 2009 *J. Am. Ceram. Int.* **35** 3067

[12] Zhou H M, Yi D Q, Yu Z M, Xiao L R and Li J 2007 *Thin Solid Films* **515** 6909

[13] Srinivasan G, Rajendra Kumar R T and Kumar J 2007 *Opt. Mater.* **30** 314

[14] Arredondo E J L, Maldonado A, Asomoza R, Acosta D R, Lira M A M, de la M and Olvera L 2005 *Thin Solid Films* **490** 132

[15] Fathollahi V and Amini M M 2001 *Mater. Lett.* **50** 235

[16] Chen K J, Fang T H, Hung F Y, Ji L W, Chang S J, Young S J and Hsiao Y J 2008 *Appl. Surf. Sci.* **254** 5791

[17] Olorunyolemi T, Birnboim A, Carmel Y, Wilson O C and Lloyd I K 2002 *J. Am. Ceram. Soc.* **85** 1249

[18] Alvarez-Quintana J, Martínez E, Pérez-Tijerina E, Pérez-García S A and Rodríguez-Viejo J 2010 *J. Appl. Phys.* **107** 063713

[19] Huang Z X, Tang Z A, Yu J and Bai S 2011 *Physica B* **406** 818

[20] Xu Y, Goto M, Kato R, Tanaka Y and Kagawa Y 2012 *J. Appl. Phys.* **111** 084320

[21] Tan Z and Di Y 2006 *Progress in Chemistry* **18** 1234

[22] Abdalla S, Easawi K, El-Brolossy T A, Yossef G M, Negm S and Talaat H 2003 *Rev. Sci. Instrum.* **74** 848

[23] Philip A, Joseph L K, Irimpan M L, Krishnan B, Radhakrishnan P, Nampoori V P N and Natarajan R 2007 *Phys. Stat. Sol. (a)* **204** 737

[24] Jothi Rajan M A, Vivekanandam T S, Radhakrishman S K, Ramachandran K and Umapathy S 2004 *J. Appl. Polym. Sci.* **93** 1071

[25] Jothi Rajan M A, Mathavan T, Vivekanandam T S and Umapathy S 2006 *J. Appl. Polym. Sci.* **100** 3756

[26] Bonno B, Laportp J and Rousset Y 1989 *J. Appl. Phys.* **67** 2253

[27] Poult P and Chambron J 1980 *J. Appl. Phys.* **51** 1738

[28] Zhan Y, Zhou X, Fua B and Chen Y 2011 *J. Hazard. Mater.* **187** 348

[29] Saber O, El-Brolossy T A and Al Jaafari A A 2012 *Water Air Soil Poll.* **223** 4615

[30] Sanchez-L Vega A, Salazar A, Ocariz A, Ponier L, Gomez W, Viuar L M and Mawcho E 1997 *Appl. Phys. A* **65** 15

[31] Raman S S, Nampoori V P N, Vallabhan C P G, Ambadas G and Sugunan S 1995 *Appl. Phys. Lett.* **67** 2939

[32] El-Brolossy T A 2012 *Indian J. Phys.* **86** 39

[33] Gadzhiev G G 2003 *High Temperature* **41** 778

[34] Wang L, Tan Z, Meng S, Liang D and Li G 2001 *J. Nanoparticle Res.* **3** 483

[35] Wang L, Tan Z, Meng S, Druzhinina A, Varushchenco R A and Li G 2001 *J. Non-Cryst. Solids* **296** 139

[36] Baletto F and Ferando R 2005 *Rev. Mod. Phys.* **77** 371

[37] Tan Z, Wang L and Shi Q 2009 *Pure Appl. Chem.* **81** 1871

[38] Tschöpe A and Birringer R 1993 *Acta Metall. Mater.* **41** 2791

[39] Zhao Y, Zhu C, Wang S, Tian J Z, Yang D J, Chen C K, Cheng H and Hing P 2004 *J. Appl. Phys.* **96** 4563

[40] Landauer R 1952 *J. Appl. Phys.* **23** 779

[41] Poulier C, Smith D S and Absi J 2007 *J. Eur. Ceram. Soc.* **27** 475